


Smart IM-MS and NMR study of natural diastereomers: the study case of the essential oil from *Senecio transiens*

Mattia Spano^{1,2} · Stéphane Andreani³ · Jean-Valère Naubron⁴ · Luisa Mannina¹ · Sabrina Pricl^{5,6} · Alain Muselli³ · Aura Tintaru² 

Abstract

Unambiguous identification of the components of a natural mixture remains a challenging and meticulous issue. Usually, different analytical techniques and laborious separation protocols are employed; nevertheless, in some cases, delicate and equivocal problems are hardly addressed by traditional methods. In this context, an original methodology for the analysis of natural samples consisting of recent mass spectrometry methods based on ion mobility (MS-IM) is proposed. As an example, a polar fraction obtained by the essential oil prepared from *Senecio transiens*, an endemic plant harvested on the Corsica Island, was selected for this study to show how IM-MS-based methods easily provide very useful insights suggesting the presence of two diastereomers. To unambiguously confirm this hypothesis and verify reliability of the IM-MS results, the purified compounds were further analysed by means of nuclear magnetic resonance (NMR) methodologies, allowing the structural elucidation and the identification of two new natural compounds, diastereomers of 4-acetoxy-5,9-dimethyl-3-(2-methylpropenyl)-2-oxabicyclo[4.4.0] dec-9-ene, reported here for the first time.

Keywords Ion mobility mass spectrometry · Essential oils · *Senecio transiens* · NMR · Vibrational and electronic circular dichroism · Density functional theory

Introduction

Wild flora constitutes a huge source of new natural compounds, which could be used primordially for pharmaceutical and medical purposes. Today, approximately 350,000 species of plants are believed to exist but only two-thirds of those have been described. Moreover, only a tiny proportion of the quarter million reported species have also been chemically characterized [1]. Secondary metabolites, broadly called natural, are obtained by different extraction methods from freshly harvested material (flowers, roots, stems, fruits, and/or leaves). Essential oils (EOs), the most studied and well-characterized class of natural mixtures, are odorous (semi)volatile compounds extracted from a single plant species by steam or hydrodistillation process or mechanical treatment. Because EOs retain the distinct odours of the natural source from which they are derived, they are named after the plant, [2] have a broad range of applications (pharmaceuticals, cosmetics, aromatherapy, and food, for example), and are of important commercial interest [1, 3].

In this context, *Senecio* is one of the largest genus in the Asteraceae family, counting more than 1500 natural species.

✉ Aura Tintaru
aura.tintaru@univ-amu.fr

¹ Department of Chemistry and Technology of Drugs, Sapienza University of Rome, Piazzale Aldo Moro 5, 00185 Rome, Italy

² Aix Marseille Univ, CNRS, UMR 7325 Centre Interdisciplinaire de Nanoscience de Marseille (CINaM), 13288 Marseille, France

³ Université de Corse, CNRS, UMR 6134 Sciences Pour L'Environnement (SPE), Laboratoire Chimie Des Produits Naturels, BP 52, 20250 Corte, France

⁴ Aix Marseille Univ, CNRS, Centrale Marseille, Spectropole, FR1739, Marseille, France

⁵ Molecular Biology and Nanotechnology (MolBNL@UniTS) Laboratory, DEA, University of Trieste, Piazzale Europa 1, 34127 Trieste, Italy

⁶ Department of General Biophysics, Faculty of Biology and Environmental Protection, University of Lodz, Lodz, Poland

Senecio is derived from the Latin word *senex*, which literally translates as “old man,” in reference to the white egrets that alight on the achenes during plant fructification [4]. Several *Senecio* species have been documented in the literature to date, some of which have a worldwide distribution (*Senecio vulgaris*), whereas others can be found only in restricted areas (e.g., *Senecio rosinae*, so far reported only on the Corsica Island). *S. transiens* is an endemic species of the Corso-Sardinian continuum [5] and, because of its regional uniqueness, this species is an important subject of investigation and further characterization.

Generally, accurate analysis of natural EOs is hardly achieved, especially when different isomers are present in the same fraction. Routinely, the chemical composition of a given EO is investigated conjointly by gas chromatography-flame ionization detector (CG-FID) and GC-mass spectrometry (MS) techniques for quantitative and qualitative purposes. Component identification is based on the comparison with data reported in the electron ionization mass spectrometry (EI-MS) spectra library. However, in many instances, a satisfactory match cannot be achieved (i.e., less than 90% of agreement), and further analyses are required. Principally, most of the ambiguities are addressed by nuclear magnetic resonance (NMR) methodologies (^1H , ^{13}C , and/or two-dimensional (2D) NMR). Nevertheless, when two or more compounds with similar structure are present in the sample, NMR analysis can be complex due to several technical issues (e.g., low signal intensity and/or significant chemical shift overlapping). In this context, the use of a complementary technique such as electrospray ionization mass spectrometry (ESI-MS) represents a promising alternative method. Recognized as a very soft ionization technique, ESI has the significant benefit of not altering the molecular structure, resulting in spectra that are substantially devoid of fragment ions, in comparison to electron ionization. Nevertheless, structural data could only be attained by tandem mass spectrometry experiments, performed post-ionization process into a collision cell, where the ions undergo controlled dissociation [6].

In the last decade, a novel technique — ion mobility mass spectrometry (IM-MS) — has been developed. Essentially, during an IM-MS experiment, ions are injected into the drift cell, where they travel through a buffer gas toward the detector under the influence of a weak electric field [7]. When two ions with the same mass-to-charge (m/z) ratio pass through the drift cell, located after the ionization source, the buffer gas will decelerate them differentially according to their active surface, also called collision cross section (CCS) [8]. Therefore, IM-MS is the method of choice when analysing isomer mixtures, for which conventional NMR and tandem mass spectrometry (MS/MS) suffer from the limitations described above, and lengthy separation and purification processes are required to obtain pure samples. When

combined with ESI-MS, IM-MS has shown high sensitivity in distinguishing isobaric species based on the difference of their CCS values [9–11].

In this work, an original and efficient combined methodology based on IM-MS and NMR techniques is proposed to investigate an isolated polar fraction of essential oils from *Senecio transiens*. This innovative approach allowed to detect and later to differentiate between two natural diastereomers, which structure is reported here for the first time. Their absolute configuration was determined using vibrational and electronic circular dichroism (VCD and ECD) spectroscopic techniques combined with density functional (DFT) calculations.

Materials and methods

Chemicals and essential oils preparation

All nondeuterated solvents were purchased from Sigma Aldrich (Saint Louis, Missouri, USA) and used without any further purification. Deuterated chloroform (99.98% D) was procured from EurIsotop (Saint Aubain, France).

Two EO samples were prepared from *S. transiens* harvested on the beaches of Calvi and Piana areas (north-west Corsica). Fresh plant material was submitted to hydrodistillation using a Clevenger apparatus under experimental conditions described elsewhere [12]. The complete GC-MS analysis of these EOs is detailed in the Supplementary Information part of the manuscript.

Purification/separative protocol

The EO from Calvi area (EO_C , 1.5 mg) was submitted to a C (CC) conducted with an increasing gradient of solvents (hexane/diethyl ether) and monitored by thin-layer chromatography (TLC) to produce 14 fractions: one apolar and 13 polar fractions were obtained. Apolar fraction was obtained by elution with 100% hexane while the polar fraction was obtained according to 8 different elution gradients (99/1%, 98/2%, 97/3%, 95/5%, 90/10%, 80/20%, 50/50%, and 0/100%). Among the polar fractions, preliminary experiments were carried out on the polar fraction, called hereafter PF_C , both eluted with 90/10 (hexane/diethyl oxide).

The EO from Piana area (EO_P , 1.5 mg) was also submitted to a silica open column chromatography according to the same methodology described above. In total, 94 fractions were eluted and after grouping by TLC fingerprints, 1 apolar and 11 polar fractions were obtained. Compounds A and B were isolated from the fraction PF_P-7 (A, 12 mg, 95%) and fraction PF_P-8 (B, 5 mg, 95%), respectively, eluted with 90/10 hexane/diethyl oxide. Progress of column chromatography (CC) was monitored by TLC as follows: TLC

was performed using silica gel 60 glass plates. 15 μL of each fraction eluted by CC (tube of collect, 10 mL) were deposited on the plate, eluted with (80/20) mixture of hexane/diethyl oxide, and revealed with solution of Cerium Ammonium Molybdate (CAM). The monitoring consists of pooling the contents of the tubes with same spots on the TLC plates to produce chemical homogeneous fractions before analysis.

NMR analysis

Samples PF_C, PF_P-7, and PF_P-8 were solubilized in CDCl₃ and analysed at 300 K using a Bruker Avance DRX 500 NMR spectrometer (Karlsruhe, Germany) operating at Larmor frequencies of 500.13 MHz and 125.76 MHz for ¹H and ¹³C, respectively, and equipped with a double resonance broadband fluorine observe (BBFO) probe (5 mm probe head). ¹H spectra were recorded using a 90° one-pulse excitation pulse sequence, 32 scans, 5 s relaxation delay, 32 k collected data points, and a spectral width of 7500 Hz (15 ppm). ¹³C spectra were recorded using a 90° one-pulse excitation pulse sequence with ¹H decoupling (WALTZ-16), 2 k up to 4 k scans basing on sample concentration, 2 s relaxation delay, 64 k collected data points, and a spectral width of 30,000 Hz (240 ppm). The residual signals of CDCl₃ (reference $\delta_{\text{H}} = 7.26$ ppm and $\delta_{\text{C}} = 77.04$ ppm) were used as references for chemical shifts. Two dimensional experiments, namely ¹H-¹H COSY (correlation spectroscopy), ¹H-¹³C HSQC (heteronuclear single quantum coherence), ¹H-¹³C HMBC (heteronuclear multiple bond correlation), and ¹H-¹H NOESY (nuclear Overhauser enhancement spectroscopy), were recorded using the same parameters previously described in the literature [13].

Mass spectrometry and ion mobility mass spectrometry

High-resolution mass spectrometry (HRMS) and IM-MS measurements were performed on a Waters Synapt HDMS II spectrometer (Manchester, UK) equipped with an ESI source and a quadrupole/time-of-flight analyser (Q-TOF). Analysed samples (PF_C, PF_P-7, and PF_P-8) were diluted (1/1000 v/v) in methanol supplemented with 1% formic acid and infused at 10 $\mu\text{L}/\text{min}$ flow rate.

ESI source was operated on positive mode using a capillary voltage of 2.8 kV. Delustering potential has been optimized at 30 V and the desolvation gas (N₂) was heated at 35 °C and introduced at 100 L/h flow. HRMS data were calibrated using clusters of sodium acetate (1 mM methanolic solution) and the MassLock protocol. The mass range was set at m/z 50 to 1500. Depending on signal intensity, each spectrum was the result of the sum of 20 to 50 recorded scans. The gas used for the mobility cell was N₂ and the main IM-MS parameters were settled as follows: travelling wave

height, WH = 23 V; travelling wave velocity, WV = 700 m/s; and IMS gas flow = 90 mL/min. Data were analysed and proceeded using MassLynx V4.2 and DriftScope programs, provided by Waters.

VCD measurements

Infrared (IR) and VCD spectra were recorded on a Bruker PMA 50 accessory coupled to a Vertex70 Fourier transform infrared spectrometer. A photoelastic modulator (Hinds PEM 90) set at 1/4 retardation was used to modulate the handedness of the circular polarized light at 50 kHz. Demodulation was performed by a lock-in amplifier (SR830 DSP). An optical low-pass filter (< 1800 cm⁻¹) before the photoelastic modulator was used to enhance the signal/noise ratio. A transmission cell equipped with BaF₂ windows and of 200 μm of optical pathlength was used. Solutions with a concentration of 0.3 mol L⁻¹ were prepared by dissolving the samples in CDCl₃. VCD spectra of samples A and B were measured at room temperature and a baseline correction was applied by subtracting the solvent spectrum. For each individual spectrum, about 12,000 scans were averaged at 4 cm⁻¹ resolution (corresponding to 3 h measurement time). For the IR absorption spectra, the cell filled with CDCl₃ was used as a reference. The spectra are presented without smoothing and further data processing.

ECD measurements

Ultraviolet–visible (UV–vis) and ECD spectra were measured on a JASCO J-815 spectrometer equipped with a JASCO Peltier cell holder PTC-423 to maintain the temperature at 20.0 °C. A quartz photoelastic modulator set at 1/4 retardation was used to modulate the handedness of the circular polarized light at 50 kHz. A quartz cell of 1 mm of optical path length was used. Solutions of A and B with a concentration of 0.0004 mol L⁻¹ were prepared in acetonitrile (HPLC grade). The CD spectrometer was purged with nitrogen during spectra acquisition. The UV absorption and ECD spectra were recorded using acetonitrile as a reference and are presented without smoothing and further data processing.

Molecular modelling/computation

Conformational study

This step has been performed using a stochastic exploration (annealing) of the potential energy surface (SEP) of the (1R,3R,4S,5R,6R)-A and (1R,3S,4R,5R,6R)-B diastereomers. For each diastereomer, the relative configuration was established through NMR. The annealing was done at the semi-empirical level (AM1) starting from a

geometry optimized using DFT with B3LYP functional and 6-311G(d,p) basis set and including solvent effects with a polarizable continuum model (SMD). During the annealing, only the dihedral angles have been relaxed while bonds lengths and valences angles were kept fixed. This step allowed for the selection of 10 conformations for each diastereomer which were then fully optimized. For VCD spectra calculations, geometries were optimized at the SMD (chloroform)/B3LYP/6-311G(d,p) level. For ECD spectra calculations, geometries were optimized at the SMD (acetonitrile)/B3LYP/6-311G(d,p) level. The resulting optimized molecular geometries were next used to calculate Boltzmann population in chloroform and in acetonitrile, respectively (see Supplementary Information). For the construction of averaged IR, VCD, UV-vis, and ECD spectra, only conformations with a Boltzmann population > 5% have been used.

Calculation of averaged IR, VCD, UV-vis, and ECD spectra

The vibrational frequencies, IR absorption, and VCD intensities were calculated using the same theoretical level adopted for geometry optimization (SMD (chloroform)/B3LYP/6-311G(d,p)). As computed harmonic frequencies were generally larger than those experimentally observed, they have been calibrated using a scaling factor of 0.98. IR absorption and VCD averaged spectra were constructed from calculated dipole and rotational strengths assuming a Lorentzian band shape with a half-width at half maximum of 8 cm^{-1} .

Based on the SMD (acetonitrile)/B3LYP/6-311G(d,p) optimized geometries, the ECD and UV spectra were calculated using time-dependent density functional theory (TD-DFT) with CAM-B3LYP functional and 6-31++G(d,p) basis set and with the SMD (acetonitrile) solvation model. Calculations were performed for vertical 1A singlet excitation using 60 states. For a comparison between theoretical results and the experimental values, the calculated UV and ECD spectra have been modelled using a Gaussian function, using a half-width of 0.37 eV. Due to the approximations of the theoretical model used, an offset almost constant was observed between measured and calculated frequencies. Using UV spectra, all frequencies were calibrated by a factor of 1.02. All calculations were performed using the Gaussian 16 package [14].

Theoretical calculations of collision cross sections

The theoretical estimation of the CCS values for the two diastereomers A and B was obtained by adapting the computational protocols based on atomistic molecular dynamics (MD) simulations described in details in our previous works [15, 16]. In brief, the two molecules were built and optimized in AMBER 20 [17] using the Generalized Amber

Force Field (GAFF) [18]. Next, each structure was immersed in a box of N_2 molecules, the resulting system was further energy-relaxed and then 200 ns of MD simulations in the isobaric-isothermal ensemble (NPT) at $T = 300 \text{ K}$ were carried out, saving trajectory frames every 0.5 ps for analysis. For CCS calculations of the Na^+ adducts of the two compounds, 20 equilibrated frames were extracted from the MD trajectories of each molecule. Then, an Na^+ ion was positioned at all possible different positions around each molecule in each extracted frame; then, the resultant complexes were geometry optimized and hence subjected to further 20 ns MD simulations by setting a mild restraint on the sodium cation to prevent its eventual “drifting.” In this way, 600 candidate structures were generated including each possible Na^+ placement and A or B diastereomers to obtain a meaningful statistical representation of the relevant CCSs. The corresponding CCS values were estimated using HPCSS, a software that performs CCS calculations based on high-performance computing (HPC) techniques [19].

Results and discussion

GC-FID and GC-MS analysis of *S. transiens* EO from Calvi area (EO_C) allowed to identify the main mixture component, namely the acetophenone derivative 3-(isopent-2-enyl)-4-methoxyacetophenone (Fig. S1). In addition, the corresponding EI-MS analysis of the peaks at 62.59 min and 63.33 min revealed the existence of two further components, both corresponding to molecular ion detected at m/z 278 and characterized by a similar EI-MS profile (Fig. 1). Interestingly, literature data survey and MS spectra library screenings did not allow any identification; accordingly, complementary analysis was performed.

Next, the polar fraction PF_C obtained by column chromatography from the EO_C sample (see “Purification/separative protocol” section) was analysed by NMR spectroscopy, and the acquired ^{13}C spectrum disclosed the presence of at least four components [20]. The major component was again the acetophenone derivative 3-(isopent-2-enyl)-4-methoxyacetophenone; its concentration was assessed to be around 80% ($\pm 0.1\%$), of the overall mixture, and its NMR values were assigned based on published data [9]. Analogously, the mixture was found to contain about 2% ($\pm 0.1\%$), of euparin [10]. The ^{13}C -NMR spectrum (Fig. 2; full ^{13}C data in Fig. S2) as well as the whole set of recorded NMR data (^1H , APT, ^1H - ^{13}C HSQC) confirmed the presence of two additional compounds (hereafter dubbed A and B), with estimated relative abundance of 7% and 10% (error: $\pm 0.1\%$), respectively. Two sets of 17 resonance were identified for the two molecules, as follows: both A and B contain one carbonyl group, four ethylenic carbons (two of which quaternary), two etheric type C-O-C moieties, four methyl

Fig. 1 Two EI-MS spectra extracted from the gas chromatogram of the *S. transiens* EO_C sample, corresponding to 62.59 min (up) and 63.33 min (down) retention time, respectively

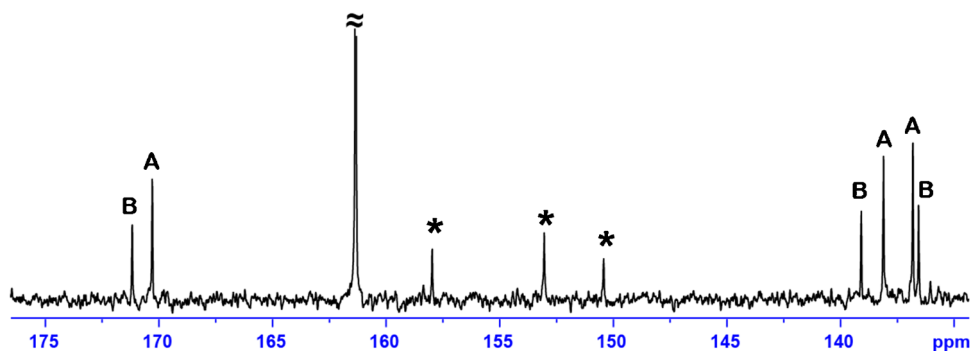
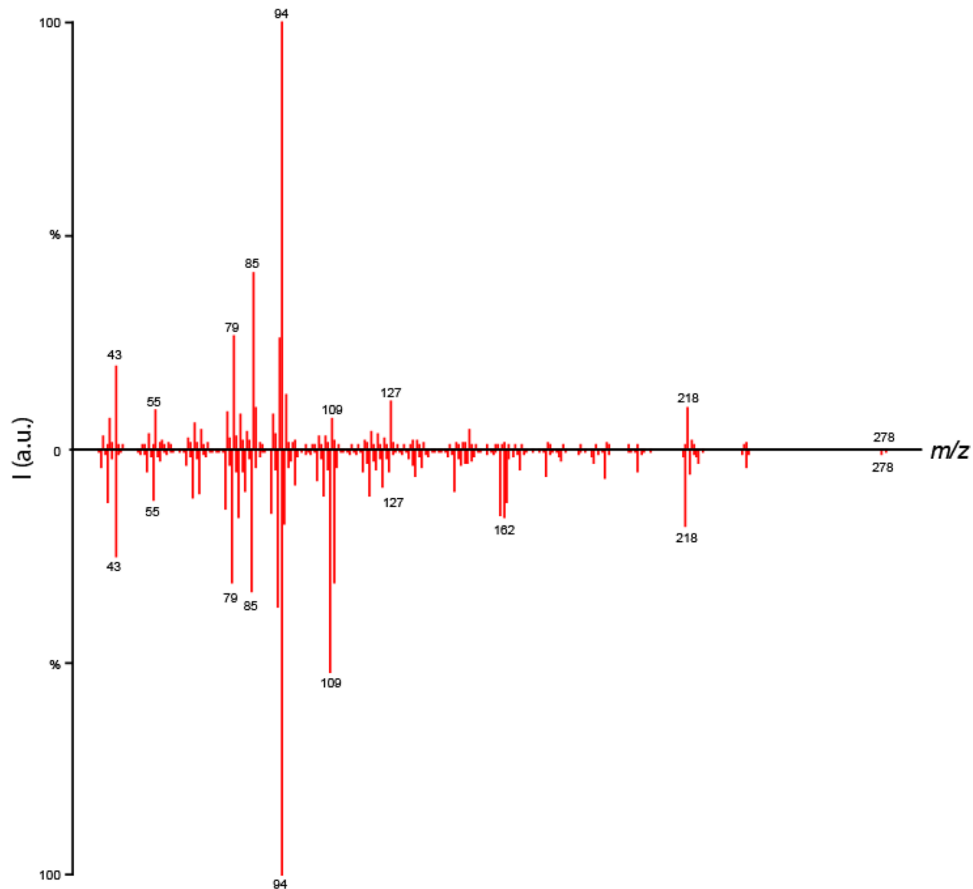


Fig. 2 Detail of the ¹³C NMR spectra (from 138 to 175 ppm) of the EO fraction showing the presence of two sets of peaks, A and B, with close chemical shift values (signals labelled with * belong to

the euparin; the resonance observed at ~162 ppm is belonging to the acetophenone derivative). The corresponding full ¹³C NMR spectrum (recorded at 125 MHz, in CDCl₃, 300 K) is reported in Fig. S2

substituents, and other sp³ methylene groups. In addition, the analysis of the ¹H NMR data showed different coupling constant for the signals corresponding to the ether groups which could be explained by the axial/equatorial positioning of the substituents (data not shown). Unfortunately, the significant signal overlap observed in the ¹H spectra precluded a straightforward unambiguous assignment and the subsequent structural identification of compounds A and

B; however, based on this information, the presence of two structural isomers or stereoisomers could be sensibly postulated (enantiomers being ruled out since they have the same NMR signals).

To get additional insights, the same fraction was further analysed by HRMS using an ESI source set on positive ionization mode. The ESI-HRMS spectrum, recorded upon ionization of the sample methanolic solution, displayed

several monocharged ions for which accurate mass measurements could be carried out. The results obtained confirmed the presence of the acetophenone derivative, which was identified at m/z 219.1385 (error 0 ppm) and m/z 241.1197 (error -0.8 ppm) in its protonated and sodiated form, respectively. Additionally, an accurate ESI (+)-HRMS spectrum (Fig. 3a) revealed the presence of another major species, identified as the sodiated cation (MNa^+), with an elemental composition of $C_{17}H_{26}O_3$ (experimental m/z 301.1776, calculated m/z 301.1774, error $+0.7$ ppm; of note, low abundant protonated species were also detected in the MS spectrum at m/z 279.1954, error -0.4 ppm). The obtained molecular formula is in excellent agreement with the structural prediction based on NMR data; moreover, the absence of any other species fully supported the presence of an isomer mixture. Unfortunately, tandem mass spectrometry is uninformative in the case of two isobaric species; therefore, separation of the mixture components was performed to proceed with further structural analysis.

Accordingly, a gas-phase separation using the ion mobility coupled with mass spectrometry was initially attempted. Surprisingly, the arrival time distribution extracted at m/z 301 revealed the presence of two isobaric molecules (Fig. 3b); yet the two species presented close drift time values and, likely, very similar structures, which did not allow for unequivocal component separation. Additionally, IM-MS/MS experiments on the mixture were carried out (Fig. S3); the corresponding fragmentation patterns obtained for each species (a priori separated into the mobility cell) were also very similar, slightly differences being observed for some fragment ion intensities, a characteristic feature reported for diastereomers [21] but not usual in the case of regio- or functional isomers [22, 23]. However, the quick IMS screening provided useful insights on the nature of the mixture under investigation, as it strongly

supported the presence of diastereoisomers in the sample, which were finally and successfully isolated via further chromatography separation.

To confirm the occurrence of diastereoisomers, both compounds A and B were isolated by successive column chromatography from the sample EO from Piana (EO_P) in two individual CC-fractions called respectively PF_P-7 and PF_P-8 (sample purity $>95\%$). The EO_P sample was chosen based on its favourable GC-profile characterized by the absence of 3-(isopent-2-enyl)-4-methoxyacetophenone, the low euparin content (8.8%), and the highest amounts of compounds A and B (15.5% and 14.3%, respectively) (Fig. S4 — Supplementary Information). Afterwards, A and B were separately analysed using NMR 1D and 2D methods (Fig. S5). Complete chemical shift assignment (Table 1) resulted in two similar molecular skeletons, both structures featuring two fused six-atom rings bearing an ethylenic moiety, an acetate group, and two CH_3 substituents; furthermore, the presence of a double bond within the bicyclic structure was also identified. These results indeed corroborated the hypothesis that A and B are diastereomeric compounds.

The peculiarity of these structures consists in the presence of five asymmetric carbons, namely C_1 , C_3 , C_4 , C_5 , and C_6 (Table 1). The proton resonances recorded for H_3 indicated a substantial difference between the two compounds ($\Delta\delta=0.51$ ppm), consistent with a conformational shift of the relevant hydrogen atom from an axial (A) to an equatorial position (B) [24–26]. Moreover, the coupling pattern of H_3 changed between the two 1H spectra; indeed, in the case of compound A, H_3 was observed as a triplet ($^3J=8.9$ Hz) whereas its resonance was seen as a doublet ($^3J=7.6$ Hz) in the 1H spectrum recorded for compound B (Fig. 4). In addition, H_4 was detected as a well-resolved triplet ($^3J=9.7$ Hz) in the 1H spectrum of compound A whereas it showed as a poorly resolved triplet ($^3J=1.8$ Hz) in the corresponding

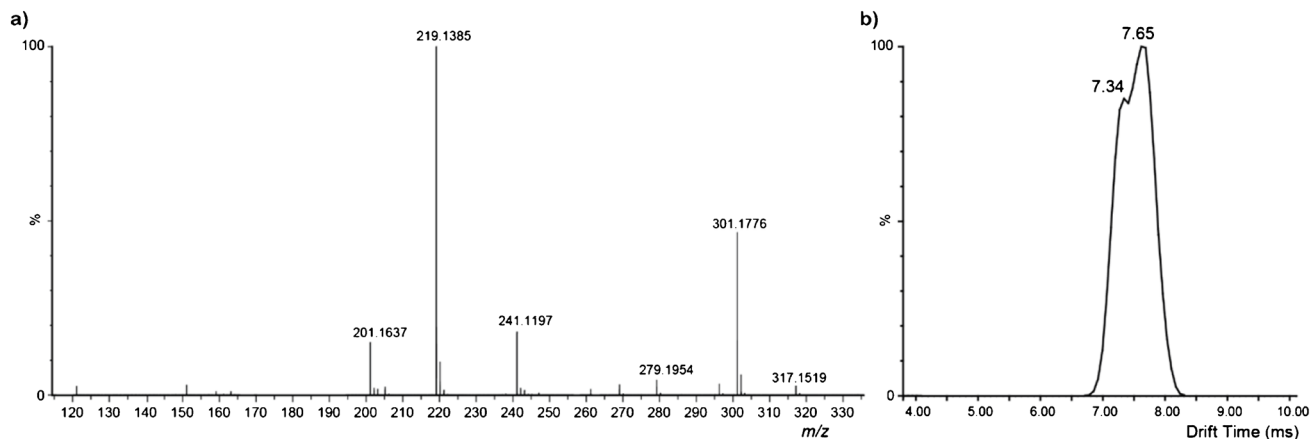
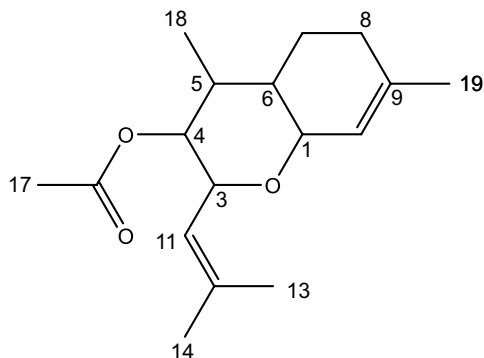


Fig. 3 **a** ESI-MS spectra of the PF_C fraction; **b** arrival time distribution extracted at m/z 301.1776 (N.B. species detected at m/z 201 correspond to an in-source fragment, $C_{15}H_{21}^+$)

Table 1 NMR data of compounds A and B (in CDCl₃, at 125 MHz and 300 K). The image shows the numbering and the molecular skeleton of two diastereoisomers

Atom No.	Compound A				Compound B			
	δ C, Type	δ H, multiplicity (<i>J</i> in Hz)	HMBC ^a	NOESY ^b	δ C, Type	δ H, multiplicity (<i>J</i> in Hz)	HMBC ^a	NOESY ^b
1	78.7, CH	3.72, m	9;10	3;5;7;10	71.8, CH	3.96, m	9;10	3;4;11;14
3	76.8, CH	4.09, t (8.9)	1;4;5;11;12;14	1;5;14	74.1, CH	4.60, d (7.6)	1;4;5;11;12	11;13
4	77.1, CH	4.54, t (9.7)	3;5;6;11;16;18	6;11;18	75.4, CH	4.69, t (1.8)	3;5;6;11;16;18	5;11;18
5	39.9, CH	1.52, m	4;6;18	1;3;18	33.3, CH	1.78, m	1;6;18	1;4;6;11;18
6	44.0, CH	1.20, m	1;5;7;18	4;7;8;18	39.4, CH	1.56, m	1;5;7	1;5;18
7	23.6, CH ₂	1.94; 1.20, m	1;5;6;8;9	1;6;8;18	23.4, CH ₂	1.86;1.15, m	1;6;8;9	1;6;8;18
8	30.5, CH ₂	2.02, m	7;9	7;19	30.7, CH ₂	2.08;1.95, m	6;9;10	7;19
9	136.8, C	NA	-	-	136.5, C	NA	-	-
10	123.0, CH	5.4, m	6;8;19	1;19	123.7, CH	5.29, m	6;8;19	1;19
11	123.0, CH	5.14, m	3;13;14	3;4;14	119.2, CH	5.45, m	3;13;14	1;3;4;5;14
12	138.1, C	NA	-	-	139.1, C	NA	-	-
13	18.7, CH ₃	1.70, d (1.3)	11;12;14	3	18.5, CH ₃	1.74, s	11;12;14	3
14	25.9, CH ₃	1.71, d (1.3)	11;12;13	11	26.1, CH ₃	1.75, s	11;12;13	11
16	170.3, C	NA	-	-	171.2, C	NA	-	-
17	20.9, CH ₃	1.98, s	16	-	21.2, CH ₃	2.10, s	16	-
18	14.2, CH ₃	0.92, d (6.4)	4;5;6	4;6;7	14.2, CH ₃	0.92, d (6.7)	4;5;6	4;5;6;7
19	22.9, CH ₃	1.66, s	8;9;10	8;10	22.9, CH ₃	1.65, s	8;9;10	8;10



^aHMBC: ¹³C-¹H long-range correlations

^bNOESY: ¹H-¹H nuclear Overhauser effect correlations

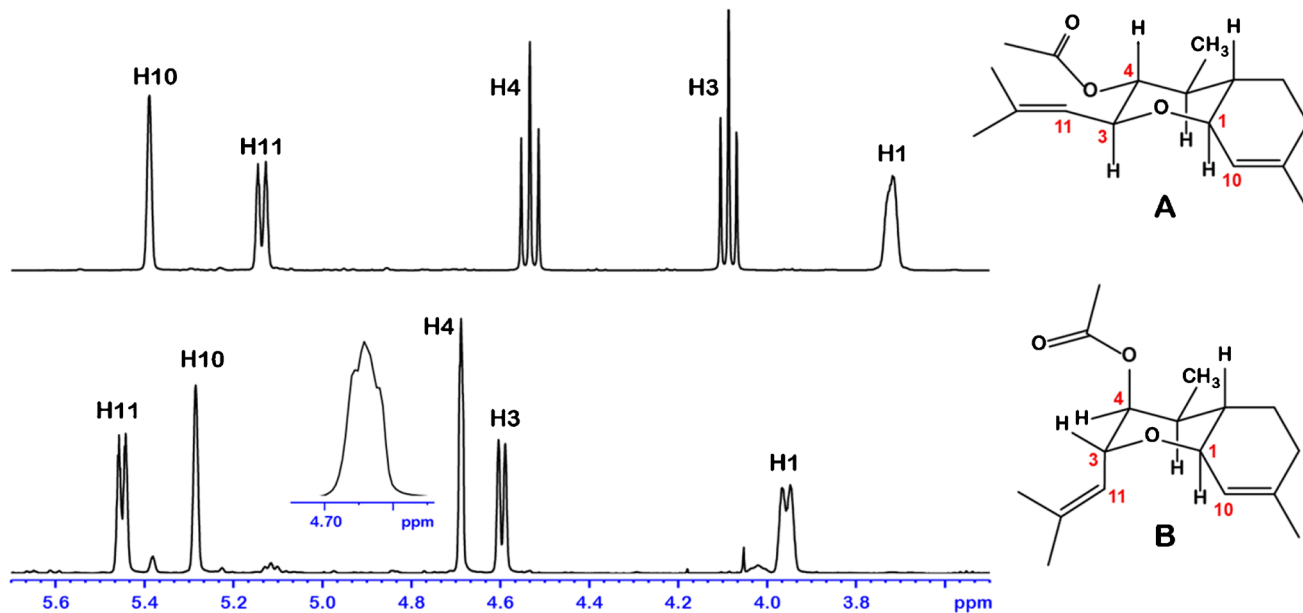


Fig. 4 Details of ^1H NMR spectra of compound A (top) and B (bottom) showing the significant changes due to the relative equatorial/axial position of H_3 , H_4 (the insert highlights the coupling pattern of

signal H_4 recorded for compound B). The structures beside show the relative position of the protons, as read from NMR data

spectrum of B (Fig. 4). Additionally, the axial/equatorial orientation of the hydrogen atoms had a significant effect on the ^{13}C signals; indeed, the chemical shift of C_3 , C_4 , and C_5 varied by more than 2 ppm between the two isomers (see Table 1). Finally, NMR data (i.e., coupling patterns, coupling constants, ^1H , and ^{13}C chemical shifts) relative to the atoms located at ring fusion (C_1 and C_6 , Table 1) revealed a *trans* configuration in both instances, owing to the axial orientation of both H_1 and H_6 , respectively [25, 27]. As a result, the stereochemistry of C_1 and C_6 in the A and B isomers is the same.

The careful analysis of nuclear Overhauser effect (NOE) cross correlation peaks further provided information on the steric configuration of the two compounds. In particular, the presence or absence of NOE cross-peaks between asymmetrical carbon hydrogens, as well as their intensity, enabled the establishment of the relative stereochemistry at each chiral centre. Thus, NOE analysis for compound A revealed an intense correlation peak between H_4 and H_6 , which was missing in compound B. In contrast, B displayed a very strong NOE between H_1 and H_{11} , that was not detected for A. The relative stereochemistry of A and B established by NMR are represented in the inset of Fig. 4; these molecular structures ultimately validate the earlier conclusions based on IM-MS that the EO extracted from the *S. transiens* plant harvested in north-west of Corsica contains two 4-acetoxy-5,9-dimethyl-3-(2-methylpropenyl)-2-oxabicyclo[4.4.0]dec-9-ene diastereoisomers. Nonetheless, studies based on vibrational circular dichroism (VCD) and electron-capture

dissociation (ECD) were further performed to determine the absolute configurations of A and B.

To establish the absolute configuration of A and B, their IR and VCD spectra were measured in deuterated chloroform and compared to the spectra calculated using DFT for selected absolute configurations. The relative configuration of the diastereomers chosen for the calculations was first established from the NMR measurements. Thus, for the simulations of the VCD spectra of compounds A and B, we selected the diastereomers (1R,3R,4S,5R,6R)-A and (1R,3S,4R,5R,6R)-B, respectively. The conformational analysis carried out for each diastereomer established that a maximum number of 3 conformations per structure was required to correctly model the IR and VCD spectra (see Supplementary Information, Figs. S6 and S7). The reduced number of conformations can be explained by the bicyclic structure and the inherent steric hindrance of these molecules. Comparison of the measured spectra with the calculated spectra showed that the absolute configurations of A and B molecules are (1R,3R,4S,5R,6R) and (1R,3S,4R,5R,6R), respectively (Figs. 5a,b). These results were lately confirmed by UV and ECD analysis. Using an approach similar to that used in VCD, the UV and ECD spectra of the diastereomers (1R,3R,4S,5R,6R)-A and (1R,3S,4R,5R,6R)-B were modelled by means of TD-DFT calculations. The calculated spectra were compared to the spectra measured in acetonitrile (see Supplementary Information, Figs. S8 and S9), and a very good agreement between measured and calculated spectra allowed to unambiguously confirm

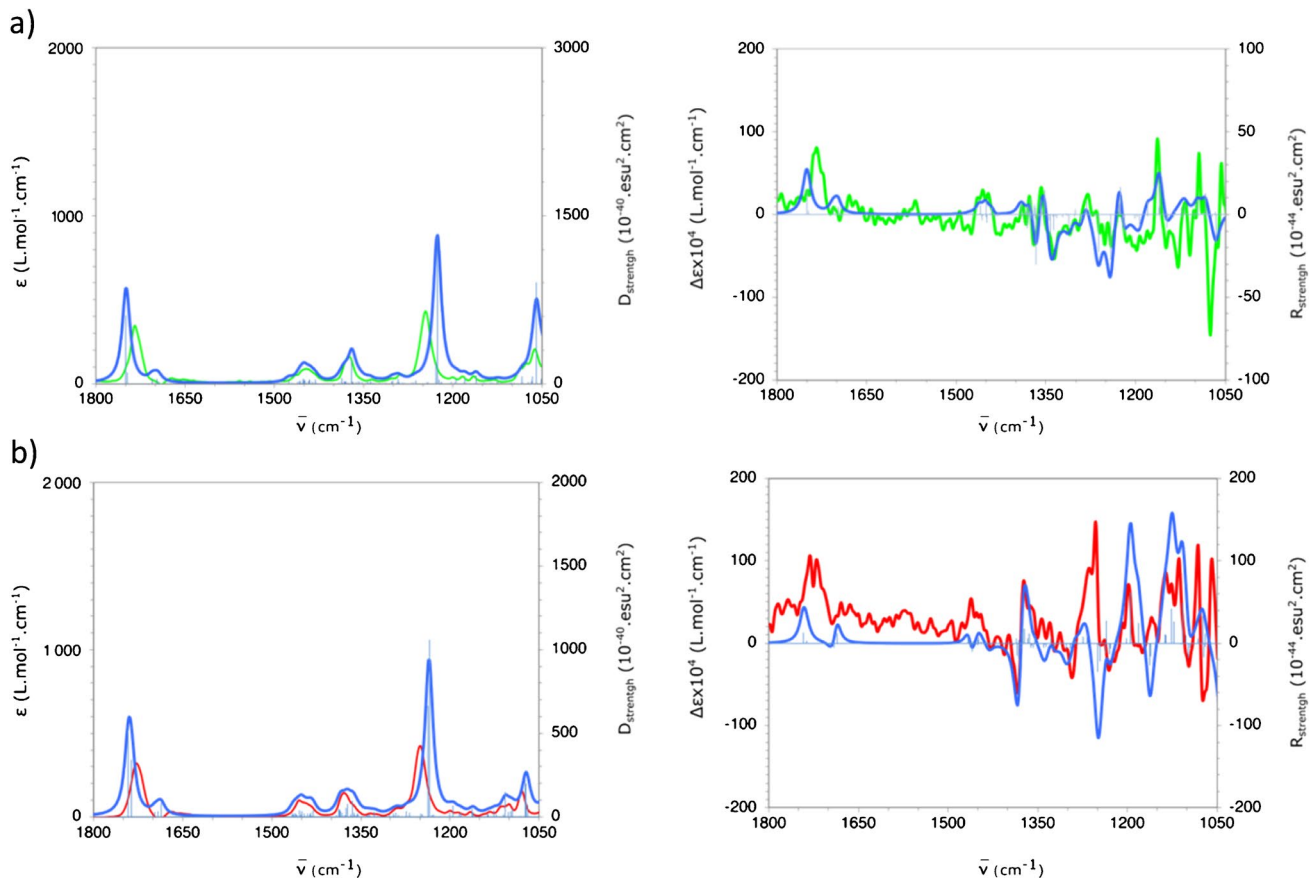


Fig. 5 **a** IR (left) and VCD (right) spectra measured in CDCl₃ for A (green) and calculated using SMD (chloroform)/B3LYP/6-311Gd,p) for (1R,3R,4S,5R,6R)-A (blue); **b** IR (left) and VCD (right) spectra

measured in CDCl₃ for B (red) and calculated using SMD (chloroform)/B3LYP/6-311Gd,p) for (1R,3S,4R,5R,6R)-B (blue)

the absolute configurations established by VCD for the molecules A and B: (1R,3R,4S,5R,6R)-4-acetoxy-5,9-dimethyl-3-(2-methylpropenyl)-2-oxabicyclo[4.4.0]dec-9-ene and (1R,3S,4R,5R,6R)-4-acetoxy-5,9-dimethyl-3-(2-methylpropenyl)-2-oxabicyclo[4.4.0]dec-9-ene, respectively. Fully VCD/ECD results and data discussion are given in the Supplementary Information of the publication.

The two purified compounds were next subjected to a more accurate IMS study. Accordingly, the arrival time distribution spectra produced for these substances validated the values of the drift times previously measured in the sample of the mixture (Table 2 and Fig. 6). Moreover, the corresponding CCS values, experimentally determined via a calibration curve obtained from poly-alanine adducts, demonstrated a considerable difference between the CCSs of the two isomers (Table 2).

As the last step in this study, we adapted a computation protocol based on atomistic MD simulations developed in our previous work to estimate the CCS values (CCS_{th}) for the two diastereomeric compounds A and B (Fig. 6). These data, listed in the last column of Table 2, are in excellent

Table 2 IM-MS values experimentally obtained and calculated at *m/z* 301 for A and B, in PF_C and purified samples, respectively. (*N.B.* CCS_{exp}=experimental CCS value; CCS_{th}=calculated CCS value, D_T=Drift time)

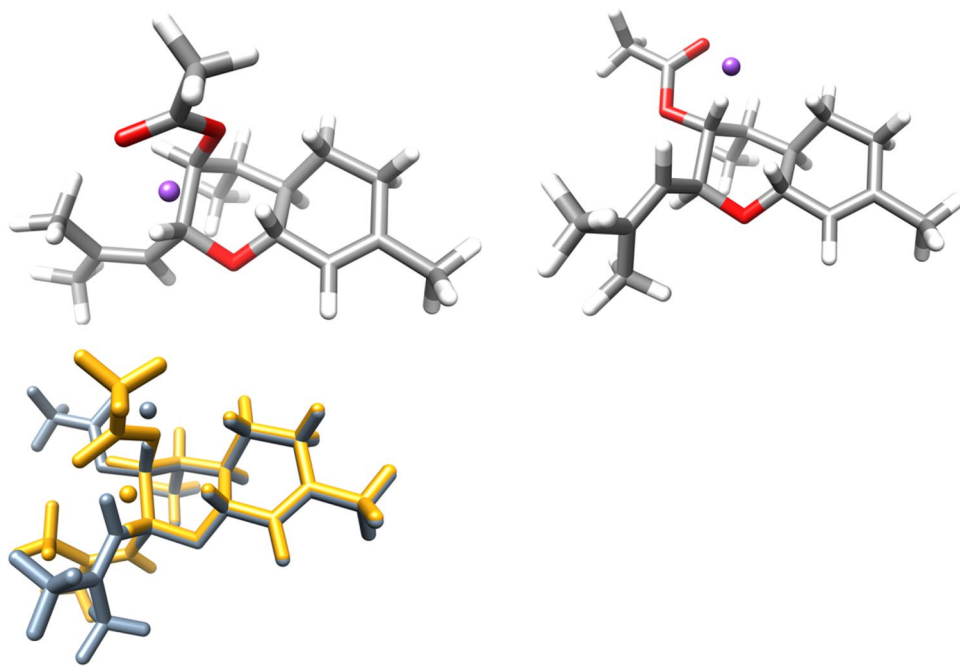
Compound	Detected ion	D _T (ms)	CCS _{exp} (Å ²)	CCS _{th} (Å ²)
A	C ₁₇ H ₂₆ O ₃ Na ⁺	7.62	191.05	190.95
A (PF _C)		7.65	191.46	
B	C ₁₇ H ₂₆ O ₃ Na ⁺	7.27	186.19	186.43
B (PF _C)		7.34	187.18	

agreement with the corresponding experimental counterparts and concur in validating the correct structural assignment of the two A and B molecules.

Conclusion

Analysis of complex matrices could be challenging, and frequently, new analytical protocols should be imagined addressing this problem. In this effort, IM-MS screening

Fig. 6 (Top) Representative images of the molecular ion $C_{17}H_{26}O_3Na^+$ for A (left) and B (right). Atoms are shown as atom-coloured sticks (C, grey, O, red, H, white), with the Na^+ ion portrayed as a purple sphere. (Bottom) Structure superposition of the molecular ions for the two compounds A (saffron) and B (faded denim)



of a complex natural fraction gave important insights on the mixture composition, ultimately predicting the presence of two diastereomers. Further purification of the fraction and successful separation of the sample constituents allow a detailed NMR analysis and full characterization of the compounds. These data confirmed our initial findings and two new natural diastereomers were discovered. VCD and ECD experiments provided the absolute stereochemistry of these diastereomers, in agreement with experimental hypothesis extracted from NMR data.

The study underlines the utility of this new IM-MS-based analytical protocol, which offers reliable results in short time and requires very small amounts of the investigated sample, as it is often the case for natural compounds. In the future, ion mobility screening of natural samples could constitute an important step during the characterization process as nature of the isomers could be established and help simplifying or even avoiding laborious separation protocols. Nevertheless, in this study, this alternative approach newly implemented for natural products investigation was combined with traditional methods to further validate the reliability of the results obtained. The good agreement found with our combined methodological approach support the systematic adoption of IM-MS methods for natural products analysis.

Supplementary Information The online version contains supplementary material available at <https://doi.org/10.1007/s00216-022-04232-y>.

Acknowledgements AT acknowledge Spectropole (FSCM FR1739) for privileged access to the instrumental park. This article is based upon work from COST Action CA 17140 — “Cancer Nanomedicine from Bench to the Bedside” supported by COST (European Cooperation in

Science and Technology). This work was supported by the computing facilities of the CRCMM, “Centre Régional de Compétences en Modélisation Moléculaire de Marseille.”

Author contribution All the authors read and approved the final version of the manuscript.

Funding This research received funding from Aix-Marseille University annual funding research support; it was not supported by any specific grant from funding agencies in the public, commercial, or not-for-profit sectors.

Declarations

Conflict of interest The authors declare no competing interests.

References

1. Cseke LJ, Kirakosyan A, Kaufman PB, Warber S, Duke JA, Briemann HL. Natural products from plants. 2nd ed. Boca Raton: CRC Press; 2006.
2. Başer KHC, Buchbauer G. Handbook of essential oils: science, technology, and applications. 3rd ed. Boca Raton: CRC Press; 2020.
3. Edris AE. Pharmaceutical and therapeutic potentials of essential oils and their individual volatile constituents: a review. *Phytother Res.* 2007;21(4):308–23.
4. Jeanmonod D, Schlüssel A, Gamisans J. Asteraceae-II. In *Compléments au Prodrome de la Flore Corse*. Genève: Conservatoire et Jardin botaniques, 2004.
5. Jeanmonod D, Gamisans J. *Flora Corsica*. Aix en Provence: Edisud, 2007.
6. Johnson AR, Carlson EE. Collision-induced dissociation mass spectrometry: a powerful tool for natural product structure elucidation. *Anal Chem.* 2015;87(21):10668–78.

7. Eiceman GA, Karpas Z, Hill HH Jr. Ion mobility spectrometry. 3rd ed. Boca Raton: CRC Press; 2013.
8. Wilkins CL, Trimpin S. Ion mobility spectrometry-mass spectrometry: theory and applications. Boca Raton: CRC Press; 2010.
9. Guo S, Zhang F, Wang H, Zhang M, Zhang Z, Zhang X, Guo Y. Behaviors of leucine and isoleucine in ion mobility-quadrupole time of flight mass spectrometry. *Chin J Chem*. 2015;33(12):1359–64.
10. Awad H, El-Aneed A. Enantioselectivity of mass spectrometry: challenges and promises. *Mass Spectrom Rev*. 2013;32(6):466–83.
11. Clowers BH, Dwivedi P, Steiner WE, Hill HH, Bendiak B. Separation of sodiated isobaric disaccharides and trisaccharides using electrospray ionization-atmospheric pressure ion mobility-time of flight mass spectrometry. *J Am Soc Mass Spectrom*. 2005;16(5):660–9.
12. Andreani S. Valorisation d'espèces envahissantes des genres *Xanthium* et *Senecio*: Caractérisation, variabilité chimique et activités des huiles essentielles. PhD Thesis. Université de CORSE - Pascal PAOLI, 2014.
13. Berger S, Braun S. 200 and more NMR experiments: a practical course. Weinheim: Wiley-VCH; 2004.
14. Frisch MJ, Trucks GW, Schlegel HB, Scuseria GE, Robb MA, Cheeseman JR, et al. Gaussian 16, Revision B.01, Gaussian, Inc., Wallingford CT GaussView 5.0. Wallingford, 2016.
15. Tintaru A, Chendo C, Wang Q, Quelever G, Peng L, et al. Conformational sensitivity of conjugated poly(ethylene oxide)-poly(amidoamine) molecules to cations adducted upon electrospray ionization—a mass spectrometry, ion mobility and molecular modeling study. *Anal Chim Acta*. 2014;808:163–74.
16. Chendo C, Moreira G, Tintaru A, Prosocco P, Laurini E, Lefay C, et al. Anomerization of acrylated glucose during traveling wave ion mobility spectrometry. *J Am Soc Mass Spectrom*. 2015;26(9):1483–93.
17. Case DA, Belfon K, Ben-Shalom IY, Brozell SR, Cerutti DS, Cheatham TE, et al. AMBER 2020, University of California, San Francisco.
18. Wang J, Wolf RM, Caldwell JW, Kollman PA, Case DA. Development and testing of a general amber force field. *J Comput Chem*. 2004;25(9):1157–74.
19. Zanotto L, Heerd G, Souza PCT, Araujo G, Skaf MS. High performance collision cross section calculation-HPCCS. *J Comput Chem*. 2018;39(21):1675–81.
20. Gerhard U, Thomas S, Mortishire-Smith R. Accelerated metabolite identification by “Extraction-NMR.” *J Pharm Biomed Anal*. 2003;32(3):531–8.
21. Wang Y, Vivekananda S, Zhang K. ESI-MS/MS for the differentiation of diastereomeric pyrimidine glycols in mononucleosides. *Anal Chem*. 2002;74(17):4505–12.
22. Tintaru A, Benchabane Y, Boyer G, Humbel S, Charles L. Differentiation of heterocyclic regioisomers: a combined tandem mass spectrometry and computational study of N-acridin-4-ylbenzylamide and N-acridin-2-yl-benzylamide. *Rapid Commun Mass Spectrom*. 2008;22(5):687–93.
23. Tintaru A, Labed V, Charles L. Structural characterisation of degradation products formed upon di-n-butyl phthalate radiolysis by high-performance liquid chromatography electrospray tandem mass spectrometry. *Eur J Mass Spectrom*. 2010;16(5):595–603.
24. Günther H. NMR spectroscopy: basic principles, concepts and applications in chemistry. 3rd ed. Weinheim: Wiley-VCH Verlag GmbH; 2013.
25. Bubb WA. NMR spectroscopy in the study of carbohydrates: characterizing the structural complexity. *Concepts Magn Resonan A*. 2003;19A(1):1–19.
26. Roslund MU, Tähtinen P, Niemitz M, Sjöholm R. Complete assignments of the ¹H and ¹³C chemical shifts and JH, H coupling constants in NMR spectra of d-glucopyranose and all d-glucopyranosyl-d-glucopyranosides. *Carbohydr Res*. 2008;343(1):101–12.
27. Kalinowsky HO, Berger S, Braun S. Carbon-13 NMR spectroscopy. Wiley; 1988.

Publisher's note Springer Nature remains neutral with regard to jurisdictional claims in published maps and institutional affiliations.

Springer Nature or its licensor holds exclusive rights to this article under a publishing agreement with the author(s) or other rightsholder(s); author self-archiving of the accepted manuscript version of this article is solely governed by the terms of such publishing agreement and applicable law.